Title

Optimization-derived blood input function using a kernel method and its evaluation with total-body PET for brain parametric imaging

Authors

Zhu, Yansong

Tran, Quyen

Wang, Yiran

et al.

Publication Date

2024-06-01

DOI

10.1016/j.neuroimage.2024.120611

Peer reviewed

HHS Public Access

Author manuscript

Neuroimage. Author manuscript; available in PMC 2024 July 16.

Published in final edited form as:

Neuroimage. 2024 June ; 293: 120611. doi:10.1016/j.neuroimage.2024.120611.

Optimization-derived blood input function using a kernel method and its evaluation with total-body PET for brain parametric imaging

Yansong Zhu[a,*], **Quyen Tran**[a], **Yiran Wang**[a,b], **Ramsey D. Badawi**[a,b], **Simon R. Cherry**[b,a], **Jinyi Qi**[b], **Shiva Abbaszadeh**[c], **Guobao Wang**[a]

[a]Department of Radiology, University of California Davis Medical Center, Sacramento, CA 95817, USA

[b]Department of Biomedical Engineering, University of California at Davis, Davis, CA 95616, USA

[c]Department of Electrical and Computer Engineering, University of California at Santa Cruz, Santa Cruz, CA 95064, USA

Abstract

Dynamic PET allows quantification of physiological parameters through tracer kinetic modeling. For dynamic imaging of brain or head and neck cancer on conventional PET scanners with a short axial field of view, the image-derived input function (ID-IF) from intracranial blood vessels such as the carotid artery (CA) suffers from severe partial volume effects. Alternatively, optimization-derived input function (OD-IF) by the simultaneous estimation (SIME) method does not rely on an ID-IF but derives the input function directly from the data. However, the optimization problem is often highly ill-posed. We proposed a new method that combines the ideas of OD-IF and ID-IF together through a kernel framework. While evaluation of such a method is challenging in human subjects, we used the uEXPLORER total-body PET system that covers major blood pools to provide a reference for validation.

[*]Corresponding author: Department of Radiology, University of California, Davis. 4860 Y Street, Sacramento, CA 95817, USA. yszhu@ucdavis.edu (Y. Zhu).

Ethics statement

All participants gave written informed consent, and all data was collected at the University of California, Davis with approval from the Institutional Review Board.

Data and code availability statements

The data and codes that support the findings of this study are available from the corresponding author upon request.

CRediT authorship contribution statement

Yansong Zhu: Writing – review & editing, Writing – original draft, Methodology, Investigation, Formal analysis, Conceptualization. **Quyen Tran:** Writing – review & editing, Methodology, Investigation. **Yiran Wang:** Writing – review & editing, Methodology. **Ramsey D. Badawi:** Writing – review & editing, Resources. **Simon R. Cherry:** Writing – review & editing, Resources. **Jinyi Qi:** Writing – review & editing. **Shiva Abbaszadeh:** Writing – review & editing, Funding acquisition. **Guobao Wang:** Writing – review & editing, Resources, Project administration, Methodology, Funding acquisition, Conceptualization.

Declaration of competing interest

UC Davis has a revenue-sharing agreement with United Imaging Healthcare. No other potential conflicts of interest relevant to this article exist.

Supplementary materials

Supplementary material associated with this article can be found, in the online version, at doi:10.1016/j.neuroimage.2024.120611.

Methods: The conventional SIME approach estimates an input function using a joint estimation together with kinetic parameters by fitting time activity curves from multiple regions of interests (ROIs). The input function is commonly parameterized with a highly nonlinear model which is difficult to estimate. The proposed kernel SIME method exploits the CA ID-IF as *a priori* information via a kernel representation to stabilize the SIME approach. The unknown parameters are linear and thus easier to estimate. The proposed method was evaluated using ^{18}F-fluorodeoxyglucose studies with both computer simulations and 20 human-subject scans acquired on the uEXPLORER scanner. The effect of the number of ROIs on kernel SIME was also explored.

Results: The estimated OD-IF by kernel SIME showed a good match with the reference input function and provided more accurate estimation of kinetic parameters for both simulation and human-subject data. The kernel SIME led to the highest correlation coefficient (R = 0.97) and the lowest mean absolute error (MAE = 10.5 %) compared to using the CA ID-IF (R = 0.86, MAE = 108.2 %) and conventional SIME (R = 0.57, MAE = 78.7 %) in the human-subject evaluation. Adding more ROIs improved the overall performance of the kernel SIME method.

Conclusion: The proposed kernel SIME method shows promise to provide an accurate estimation of the blood input function and kinetic parameters for brain PET parametric imaging.

Keywords

Tracer kinetic modeling; Input function estimation; Kernel method; Total-body PET

1. Introduction

Positron emission tomography (PET) has been widely applied in clinical and research scenarios. Compared to static PET, dynamic PET allows more accurate quantification of different physiological processes using tracer kinetic modeling (Wang et al., 2020; Gallezot et al., 2020). An accurate blood input function is essential to perform tracer kinetic analysis. Conventionally, the blood input function is obtained by arterial catheterization. This method, however, is invasive and requires extra processing time (Feng et al., 2020).

Noninvasive or less invasive methods for obtaining blood input functions have attracted much research interest (van der Weijden et al., 2023; Bartlett et al., 2022). For example, a population-based input function can be obtained from a cohort of subjects, and is then scaled for individual subjects (Takikawa et al., 1993; Eberl et al., 1997). However, such a method may not be adaptive enough to individual subjects due to its fixed shape. The image-derived input function (ID-IF) is another category of noninvasive methods. An ID-IF can be extracted from large blood pools such as the ascending aorta or left ventricle (der et al., 2001; de et al., 2006). However, these major blood pools are not always covered in the field of view (FOV), such as in brain or head & neck imaging using conventional short PET scanners (Feng et al., 2012; Mourik et al., 2008). As a result, an ID-IF often has to be extracted from small blood vessels such as the carotid arteries, which suffer from severe partial volume effect (Zanotti-Fregonara et al., 2009; Volpi et al., 2023). Although multiple studies have applied partial volume correction during extraction of the ID-IF (Mourik et al., 2008; Croteau et al., 2010), these methods are sensitive to the accuracy of system

point-spread-function estimation and the precision of vessel segmentation. Alternatively, an optimization-derived input function (OD-IF) can be obtained using the simultaneous estimation (SIME) method which seeks to estimate the input function jointly with kinetic parameters by fitting time activity curves (TACs) from multiple regions of interest (ROIs), e.g. (Feng et al., 2020, 1997; Ogden et al., 2010; Wong et al., 2002; Samil Yetik and Qi, 2006). While the performance of SIME was evaluated on different tracers (Bartlett et al., 2019; Zanderigo et al., 2018; Guo et al., 2007; Sari et al., 2018), conventional SIME parameterizes the input function using a highly nonlinear model and the optimization problem is complex to solve, either requiring a sophisticated optimization algorithm (e.g., (Wong et al., 2002)) or the model fitting may easily fail, as demonstrated later in the supplement. In addition, the model of the input function is challenging to match well with the specific data of the subject, especially for the early time period after injection (Yi-Gen, 2008; Wong et al., 2006). Combining ID-IF with OD-IF provides a way to address the challenge of SIME. Constrained SIME methods (e.g., (Sari et al., 2018)) were proposed previously by utilizing the information from an image-derived whole-blood curve, but the model of the input function remains nonlinear and the application was mainly for metabolite correction by assuming the whole-blood curve is correct (Sari et al., 2018).

In this work, we further explore the ideas of ID-IF together with OD-IF to address the challenge of SIME without assuming a perfect whole-blood curve. A kernel SIME method is developed by exploiting the ID-IF as a priori information to stabilize SIME using a linear kernel representation of the input function. The method was evaluated using ^{18}F-fluorodeoxyglucose (FDG) with both a computer simulation study and human-subject data. Evaluating such a method in human subjects is generally challenging because arterial blood samples are normally required to provide the reference truth. Here we leveraged the uEXPLORER total-body PET system (Cherry et al., 2018; Badawi et al., 2019; Zhang et al., 2020) to extract the reference from major blood pools for validation.

2. Methods

2.1. Tracer kinetic modeling

A commonly used two-tissue (2T) model for dynamic ^{18}F-FDG PET is (Dimitrakopoulou-Strauss et al., 2021):

$$\frac{d}{dt}\begin{bmatrix}C_f(t)\\C_m(t)\end{bmatrix}=\begin{bmatrix}-(k_2+k_3) & k_4\\ k_3 & -k_4\end{bmatrix}\begin{bmatrix}C_f(t)\\C_m(t)\end{bmatrix}+\begin{bmatrix}K_1\\0\end{bmatrix}C_p(t), \tag{1}$$

where $C_p(t)$ is the input function that represents the FDG concentration in plasma. $C_f(t)$ and $C_m(t)$ are the free and metabolized FDG concentrations, respectively. K_1, k_2, k_3, and k_4 are the tracer rate constants. The solution of this equation gives the total activity of FDG in the extravascular space as:

$$C_t(t)=C_f(t)+C_m(t)=h(t)\otimes C_p(t), \tag{2}$$

where ⊗ denotes convolution, and $h(t)$ is the impulse response function given by

$$h(t) = \frac{K_1}{\Delta\alpha}[(k_4 - \alpha_1)e^{-\alpha_1 t} + (\alpha_2 - k_4)e^{-\alpha_2 t} + k_3(e^{-\alpha_1 t} - e^{-\alpha_2 t})], \tag{3}$$

where $\Delta\alpha = \alpha_2 - \alpha_1$, $\alpha_{1,2} = \frac{1}{2}(k_2 + k_3 + k_4) \mp \frac{1}{2}[(k_2 + k_3 + k_4)^2 - 4k_2k_4]^{\frac{1}{2}}$. The observed total tissue activity $C_T(t)$ is:

$$C_T(t) = (1 - v_b)C_t(t) + v_bC_{wb}(t) = (1 - v_b)h(t) \otimes C_p(t) + v_bC_{wb}(t), \tag{4}$$

where v_b is the fractional volume of blood in the tissue. $C_{wb}(t)$ is the tracer concentration in the whole blood and is related to $C_p(t)$ with the plasma-to-blood ratio (PBR) function as

$$C_p(t) = \mathrm{PBR}(t)C_{wb}(t)\,. \tag{5}$$

A nonlinear model for PBR function, $\mathrm{PBR}(t) = 1 / [0.97 - 0.06\exp(-0.085t)]$, where t is in the unit of min, was applied in this work (Naganawa et al., 2020; Zuo et al., 2021).

2.2. Conventional SIME

The conventional SIME method exploits the assumption that TACs from different ROIs share the same input function (Feng et al., 2020). Thus, the input function can be estimated jointly with kinetic parameters by fitting TACs from multiple ROIs (Feng et al., 1997). The cost function for conventional SIME is:

$$\Phi(\boldsymbol{\theta}, \boldsymbol{C}_p) = \sum_{j,m} w_j[C_{T,j}(t_m; \boldsymbol{\theta}_j, \boldsymbol{C}_p) - c_j(t_m)]^2, \tag{6}$$

where $c_j(t_m)$ is the measured TAC for j^{th} tissue ROI and m^{th} time frame. The weighting factor w_j is computed as $w_j = 1 / \left(\frac{1}{M}\sum_m c_j(t_m)\right)^2$ to normalize the scale of TACs from different regions, with M as the total number of time frames. $\boldsymbol{\theta}_j = \{v_{b,j}, K_{1,j}, k_{2,j}, k_{3,j}, k_{4,j}\}$ are kinetic parameters to be estimated, and $\boldsymbol{C}_p$ is the unknown plasma input function vector. Here the model TAC $\boldsymbol{C}_T$ is explicitly written as a function of $\boldsymbol{C}_p$ and kinetic parameters $\boldsymbol{\theta}$. Note that the whole-blood function $C_{wb}(t)$ in Eq. (4) is in turn denoted by $C_{wb}(t) = C_p(t) / \mathrm{PBR}(t)$. In this work for ^{18}F-FDG studies, we initialized $\boldsymbol{\theta}$ as [0.1, 0.1(mL/min/cm^3), 0.1(min^{-1} 0.1(min^{-1}), 0.01(min^{-1})]^T, and the lower bound was 0 and the upper bound was [1, 2(mL/min/cm^3), 2(min^{-1}), 2(min^{-1}), 0.5(min^{-1})]^T. The input function was converted to standard uptake values (SUV) and the upper and lower bound was set as 120 and 0, respectively.

Often, the input function is parameterized using Feng's model (Feng et al., 1994). One challenge for SIME with Feng's model is that both the kinetic modeling and the input function models are nonlinear, and the optimization problem is complex and often demonstrates instability in practice. Supplemental Fig. 1 shows an example that the SIME with the Feng's model fails to estimate the input function accurately with simulation data, which is due to the local optimum in a highly nonlinear optimization problem. Alternatively, the input function $\boldsymbol{C}_p$ can be directly estimated as time points without using a nonlinear model, which however may result in a noisy estimation. For SIME methods, at least one reference point is required in order to overcome the global scaling problem (Ogden et al., 2010; Guo et al., 2007; Riabkov and Di Bella, 2002; Riabkov and Bella, 2004).

2.3. Kernel SIME

While an ID-IF from a small blood region does not provide an accurate input function, the extracted ID-IF may already include useful *a priori* knowledge, such as the temporal correlations of different time points of the true input function. Inspired by the kernel method for tomographic image reconstruction (Wang and Qi, 2015; Wang, 2019), here we propose a kernel SIME method to utilize the *a priori* information from ID-IF through a kernel representation to describe the input function at the time frame m:

$$C_{p,m} = \sum_n \alpha_n \kappa(\boldsymbol{f}_m, \boldsymbol{f}_n), \tag{7}$$

where α_n is the kernel coefficient for n^{th} time frame. $\boldsymbol{f}_m$ and $\boldsymbol{f}_n$ are 3×1 1D feature vectors extracted from ID-IF that centered at m^{th} and n^{th} time frame, respectively. $\kappa(\boldsymbol{f}_m, \boldsymbol{f}_n)$ is a kernel function and can be computed using radial Gaussian kernel as (Wang and Qi, 2015):

$$\kappa(\boldsymbol{f}_m, \boldsymbol{f}_n) = \exp\left(-\frac{\|\boldsymbol{f}_m - \boldsymbol{f}_n\|^2}{2\sigma^2}\right), \tag{8}$$

where σ is a hyper parameter and is set as 1 in this study. Supplemental Fig. 2 illustrates how to obtain the kernel function from an ID-IF. With this kernel representation, the input function is now expressed as a linear matrix-vector form $\boldsymbol{C}_p = \boldsymbol{K}\boldsymbol{\alpha}$, where $\boldsymbol{K}$ is the kernel matrix with its $(m, n)^{\text{th}}$ element as $\kappa(\boldsymbol{f}_m, \boldsymbol{f}_n)$. Note that the kernel representation here is nonlinear with respect to the feature vectors which embed the prior information, but is linear with respect to the unknown model parameter $\boldsymbol{\alpha}$, leading to an easier optimization problem as compared to a highly nonlinear model. Accordingly, the cost function in Eq. (6) becomes:

$$\Phi(\boldsymbol{\theta}, \boldsymbol{\alpha}) = \sum_{j,m} w_j [C_T(t_m; \boldsymbol{\theta}_j, \boldsymbol{K}\boldsymbol{\alpha}) - c_j(t_m)]^2 \tag{9}$$

To minimize the cost function in Eq. (9), the classic Levenberg-Marquardt algorithm used in tracer kinetic modeling was applied and implemented using MATLAB (MathWorks). The ID-IF was used as the initial guess for estimating $\boldsymbol{\alpha}$.

2.4. Evaluation with simulation study

A computer simulation study was conducted to evaluate the proposed method. TACs from the ascending aorta (AA) and carotid artery (CA) were extracted from the total-body dynamic FDG scan of a human subject on a uEXPLORER PET/CT system that lasted one hour with the following framing: 12 × 5 s, 4 × 15 s, 2 × 30 s, 3 × 60 s, 8 × 180 s, 6 × 300 s. Image from 20 to 25 s was used to place ROIs for AA and CA since the blood vessels can be clearly visualized from this time frame. To extract TAC from AA, an ellipsoid ROI with a dimension of 20 × 40 × 20 mm^3 was placed (see supplemental Fig. 5c, 5d). The blood TAC from AA was used as the true input function in this study. TAC from CA was extracted by manually segmenting CA from the 20–25 s PET image (see supplemental Fig. 5a, 5b). TACs from four brain regions were simulated, including gray matter (GM), white matter (WM), cerebrospinal fluid (CSF), and cerebellum. The simulated kinetic parameters were obtained by taking the average kinetic parameters from a dataset consisting of 20 real human subjects, as summarized in Table 1. Time-varying Gaussian noise was added to the brain TACs following the method described in (Zuo et al., 2018), with the noise standard deviation SD_m for the m^{th} frame defined as:

$$SD_m = S_c\sqrt{c_m \exp(\lambda t_m) \,/\, \Delta t}, \tag{10}$$

where λ is the decay constant of ^{18}F-FDG, c_m is the noise-free TAC for the m^{th} frame. t_m and Δt_m are the middle time and the scan duration of frame m, respectively. S_c is a scaling factor to match the simulated noise level to that of the realistic dynamic FDG data (Zuo et al., 2018). S_c was chosen as 1.47 in this simulation study of dynamic brain FDG-PET. The simulation was repeated for 20 different noise realizations. We compared our proposed kernel SIME with the conventional SIME, and the CA-extracted ID-IF. Supplemental Fig. 3 shows the flowcharts of the three methods to illustrate their relationships and differences. For all the methods, the last time point was scaled to the true input function to overcome the scaling problem. For quantitative evaluation, bias and standard deviation of kinetic parameters were computed as:

$$\text{Bias} = \left| \frac{\bar{x} - x_t}{x_t} \right| \times 100\,\%, \tag{10a}$$

$$\text{Std} = \sqrt{\frac{1}{N-1}\sum_{i=1}^{N}(x_i - \bar{x})^2} \tag{11}$$

where x is the estimated kinetic parameter, x_t is the ground truth, $\bar{x} = \frac{1}{N}\sum_{i=1}^{N} x_i$ is the mean of x, N is the number of noise realizations. In this work, for both the simulation study and human-subject study described in the next section, we used AMIDE software for ROI placement, TAC extraction and image display purposes (Loening and Gambhir, 2003). Quantitative analysis and display of quantitative results were performed with MATLAB (MathWorks).

2.5. Evaluation with total-body dynamic FDG scans

We then evaluated our proposed method on a dataset consisting of 10 healthy subjects and 10 cancer patients acquired on the uEXPLORER total-body PET/CT system. The demographic characteristics of the 20 subjects are summarized in Table 2. Each subject was injected with ~370 MBq (10 mCi) ^{18}F-FDG, followed by a 60-minute total-body dynamic PET scan with the same framing as the simulation study. Each frame was reconstructed into an image of size 150 × 150 × 486 with 4 × 4 × 4 mm^3 voxels using the vendor implementation of the time-of-flight ordered-subset expectation maximization algorithm with 4 iterations and 20 subsets (Spencer et al., 2020).

Six brain TACs were extracted, including GM, WM, CSF, cerebellum, brain stem and thalamus. The averaged TACs for each ROI are shown in supplemental Fig. 4. TACs from AA and CA were extracted by placing ROIs using PET images from early frames, as shown in supplemental Fig. 5. AA TACs were used as the reference truth of the blood input function in this study.

We first compared the proposed kernel SIME with the conventional SIME and the CA ID-IF. For this part, 4 brain TACs (GM, WM, CSF, cerebellum) were first used for SIME methods. The effect of the number of ROIs on kernel SIME was also studied. For both studies, the last time point was scaled to the reference input function for all the methods. The time delay effect was also modeled. Given the difference of time delay between different brain regions is relatively small, we modeled a global time delay parameter in the blood input function and estimated this parameter through a grid search method as described in (Wang et al., 2022). To quantitatively evaluate the estimated input functions, the area under curve (AUC) ratio (Zanotti-Fregonara et al., 2011) and the mean absolute error (MAE) was computed as:

$$\mathrm{AUC}_{\mathrm{ratio}} = \frac{\int C_{p,est}(t)dt}{\int C_{p,ref}(t)dt}, \tag{12}$$

$$\mathrm{MAE} = \frac{\sum_{m=1}^{M} \mid C_{p,est}(t_m) - C_{p,ref}(t_m) \mid}{\sum_{m=1}^{M} C_{p,ref}(t_m)} \times 100\ \%, \tag{13}$$

where $C_{p,est}$ and $C_{p,ref}$ are estimated and reference input functions, respectively. M is the total number of time frames. We then evaluated the quantitative accuracy of FDG delivery rate

K_1, fractional blood volume v_b, and net influx rate $K_i = K_1 k_3 / (k_2 + k_3)$ obtained with different input functions. Reference kinetic parameters were obtained by using the reference input function for kinetic modeling. MAE and the Pearson correlation coefficient were computed between an estimated kinetic parameter and its reference value.

To visualize the effect of different input functions on kinetic parameter estimation, we generated parametric images for the brain with an isotropic voxel size of 2.3 mm for a better image resolution. The parametric images were generated by voxel-wise TAC fitting with input functions from different methods.

3. Results

3.1. Simulation study

Fig. 1 shows the results of the estimated input function obtained by different methods. Both the kernel SIME and conventional SIME showed improvement for peak estimation as compared to the ID-IF. Compared to conventional SIME, kernel SIME showed a better match with the true input function. The results of fitted TACs in different brain regions are shown in supplemental Fig. 6. Interestingly all the methods were able to fit the tissue TACs well.

Fig. 2 further shows the estimated K_1, K_i and v_b values for different ROIs with different methods. Overall, the kernel SIME provided the most accurate estimation results as compared to the ID-IF and conventional SIME methods. Among all the three methods, the ID-IF led to the highest bias in K_1 (83.3 % averaged over all brain ROIs) and v_b (average bias of 189.5 %). Compared to ID-IF, conventional SIME resulted in a lower bias for K_1 (average bias of 40.7 %) and v_b (average bias of 125.8 %), but the noise is much higher than the other two methods. The kernel SIME had the lowest bias for K_1 (average bias of 3.6 %) and v_b (average bias of 26.9 %) among the three methods. The percent bias in v_b was large in part due to its small absolute value in the brain regions. All the three methods were able to generate relatively accurate estimation for K_i,

3.2. Total-body dynamic FDG data

3.2.1. Comparison between different methods—We first compared the results from our proposed kernel SIME with the conventional SIME and CA ID-IF methods. Fig. 3 shows an example of the estimated input functions with different methods. The results of average AUC ratios and MAEs are shown in supplemental Table 1. The kernel SIME led to a substantial improvement compared to the other two methods and a better match with the reference input function, especially for the early phase. It also had the highest AUC ratio (0.935 ± 0.111) and the lowest MAE (16.4 % ± 5.6 %) among all the methods. Higher standard deviations are observed for results of the conventional SIME, indicating that it is sensitive to the noise in TAC data.

Fig. 4 shows the scatter plots of the estimated kinetic parameters vs. reference kinetic parameters for different methods. The quantitative results are summarized in Table 3. For all the three kinetic parameters, the results by ID-IF and conventional SIME deviated

from the reference values, indicating that biases were induced by these two methods. In comparison, the estimated kinetic parameters by the kernel SIME matched the reference values well. We observed that the estimated kinetic parameters from kernel SIME had the lowest MAEs among the three methods. Compared to the ID-IF method, the conventional SIME had lower MAEs for K_1 and v_b, but also with the lower correlation coefficients for all three kinetic parameters. This observation is consistent with its unstable performance in estimating the input function. In this human-subject study, we observed the ID-IF method and the conventional SIME method generate a larger error for K_i estimation as compared to the results from the simulation study. This could be caused by the heterogeneity of human subjects, while the simulation study was conducted based on one subject. To illustrate the effect of individual subject differences on K_i estimation, supplemental Fig. 7 shows the results from a simulation study that used the TAC data extracted from a different subject. In this case, ID-IF and the conventional SIME methods have a larger error on K_i estimation compared to the results shown in Fig. 2. The proposed method still provided the best performance.

Figs. 5, 6 and supplemental Fig. 8 show K_1, K_i and v_b images obtained with the input functions from different methods, respectively. The asymmetric brain structures shown in the coronal slices were caused by the head rotation of the subject, as can be seen from the transverse slices. The images from kernel SIME were similar to the reference images. In comparison, the CA ID-IF resulted in overestimation in all three parametric images. Conventional SIME showed overestimation for K_i and v_b images and underestimation for K_1 images.

3.2.2. Influence of the number of ROIs—We performed kernel SIME with tissue TACs from 2 ROIs (GM, WM), 3 ROIs (GM, WM, and CSF), 4 ROIs (GM, WM, CSF, and cerebellum), 5 ROIs (GM, WM, CSF, cerebellum, and thalamus), and 6 ROIs (GM, WM, CSF, cerebellum, thalamus, and brain stem) that consist of typical brain regions. The AUC ratios and MAEs of the input functions estimated with different numbers of ROIs were shown in supplemental Table 2. Overall, we observed an increasing trend for AUC ratio and a decreasing trend for MAE as more ROIs were applied for the joint estimation. Fig. 7 shows the effect of more ROIs on the final kinetic parameter quantification according to the correlation coefficient and MAE, which were computed by averaging results from GM and WM for all the 20 subjects. While two ROIs (GM, WM) were too few, the four-ROI option (GM, WM, CSF, and cerebellum) provided good results (about an average MAE of 10 % and correlation coefficient of 0.97). Adding extra ROIs from the thalamus and brain stem did not improve the results dramatically.

4. Discussion

In this work, we developed a method for optimization-derived blood input function. The method can be generally applied when the major blood pools are not covered in dynamic PET imaging. The method was evaluated using both simulation data and human-subject brain data collected from the uEXPLORER total-body scanner, which provides simultaneous coverage of major blood pools to extract a cardiac ID-IF as the reference for validation of

our method. The method shows promise to be applied for brain parametric imaging with conventional short scanner or dedicated brain scanner (Catana, 2019). While the evaluation was focused on brain imaging in this work, we believe the method can also be extended to other applications such as head & neck cancer imaging and rectal cancer imaging (Thorwarth et al., 2005; Strauss et al., 2007) for which it is usually challenging to extract a good ID-IF due to the absence of a major blood pool in the FOV of conventional PET scanners.

Our proposed kernel SIME method demonstrates superior performance compared to the conventional SIME method and the CA ID-IF. The conventional SIME showed unstable performance due to the highly challenging optimization problem (Fig. 2, supplemental Table 1). The incorporation of prior information from the ID-IF by the kernel method helped stabilize and improve the performance of SIME. Specifically, the proposed method substantially improved the estimation of the early time points of the input function (Figs. 1, and 3). This in turn helped improve the estimation of K_1 and v_b as they are more sensitive to the shape of the early phase of the input function (Zanotti-Fregonara et al., 2009; Wahl et al., 1999). This was further validated by the results of estimated kinetic parameters (Figs 4–6).

We further evaluated our proposed method with different number of ROIs. Overall, using more ROIs improves both the estimated input function and kinetic parameters (Fig. 7, supplemental Table 2). Early work by others shows that at least three ROIs (of distinct shapes) are required for a unique solution of SIME problem using two-tissue model (Riabkov and Bella, 2004). TACs with similar shapes might contribute less to help the estimation, as shown in supplemental Fig. 4, while smaller ROIs may induce higher noise. These factors could influence the selection of ROIs for estimation. In this study for brain imaging, we observed that using 4 ROIs (GM, WM, CSF, and cerebellum) could provide a good performance, offering an appropriate choice in practice.

As an initial demonstration, the proposed method was evaluated for the widely used radiotracer FDG. Other tracers such as amyloid tracers and tau tracers have also received much interest in brain PET imaging for Alzheimer's disease (Landau et al., 2014; Kolanko et al., 2020; Saint-Aubert et al., 2017; Okamura et al., 2018). While an ID-IF generally requires an additional metabolite correction step for these tracers, an advantage for the proposed SIME method for OD-IF is that it theoretically allows the estimation of metabolite-corrected input function (Gallezot et al., 2020). On the other hand, these tracers may have different kinetic properties compared to FDG, resulting in very different shape of tissue TACs. In general, the proposed method could work so long as the CA ID-IF contains the shape information of the plasma input function. In practice, the detailed effects of different shapes of tissue TACs and CA ID-IF may be different and need to be further studied for individual radiotracers. We will explore the performance of the proposed method with these tracers in future work.

Some limitations exist in this work. All the SIME methods, including the proposed method, require scaling of the estimated input function using a known blood activity, e.g., from a late time point. Conventionally this would require one invasive blood sample in practice (Ogden et al., 2010). However, this still reduces the effort compared to the case that

requires multiple arterial blood samples to be obtained and analyzed. This might bring potential application for applying this method on the new generation brain PET scanner for parametric imaging. Furthermore, such a measurement of blood input at a late time point can be directly extracted from a separate scan of the heart, which may be acquired when performing whole-body static imaging for oncological applications. Such a scan protocol where a dynamic brain scan is followed by a whole-body static scan may have potential to enable brain parametric imaging in cancer patients, which may have various clinical applications such as for quantitative study of chemo brain. Another limitation of this work is that instead of using arterial blood samples as reference standard, which is common in many other works, we used the AA ID-IF obtained with total-body PET as the reference. We consider this as a reasonable alternative as the AA ID-IF has been shown to provide a good approximation to the arterial input function (der et al., 2001), though some differences could exist between the two functions. On the other hand, arterial blood sampling is not without problems, for example, external delay and dispersion effects need to be considered due to sampling from peripheral arteries and inhomogeneous velocity in the vessels and the catheter (Dimitrakopoulou-Strauss et al., 2021). Lastly, the CA ID-IF was used in the comparison study without partial volume correction, which might only represent a sub-optimal performance for CA ID-IF. Even with partial volume correction, the corrected CA ID-IF may still lead to inaccurate quantification for microkinetic parameters, such as K_1 (Providência et al., 2024). While partial volume correction is not a trivial task (Mourik et al., 2008; Croteau et al., 2010), an advantage of the proposed method is that it can be applied to the uncorrected CA ID-IF directly as the estimation may correct for partial volume effect at least in part.

5. Conclusion

We developed a kernel SIME method that exploits ID-IF as *a priori* information to estimate the blood input function from imaging data. Results from simulation study and human-subject dataset indicate that compared with the CA ID-IF and conventional SIME methods, our proposed method substantially improves the estimates of the input function, especially for the early time points, and the accuracy of the estimated kinetic parameters. Overall, our method shows promise when an accurate ID-IF cannot be obtained from major blood pools. This method may have a number of potential applications, including brain parametric imaging with dedicated brain scanner or non-invasive studies of chemo brain in cancer patients in combination with whole-body imaging.

Supplementary Material

Refer to Web version on PubMed Central for supplementary material.

Acknowledgements

The authors thank Drs. Kevin J. Chung and Benjamin A. Spencer for help to reconstruct the dynamic image data used in this study.

Disclosure

This work was supported by NIH R01EB028091, R01 CA206187 and R01 EB033435. UC Davis has a revenue-sharing agreement with United Imaging Healthcare. No other potential conflicts of interest relevant to this article exist.

Data availability

Data will be made available on request.

References

Badawi RD, Shi H, Hu P, et al. , 2019. First human imaging studies with the EXPLORER total-body PET scanner*. J. Nucl. Med 60 (3), 299–303. 10.2967/jnumed.119.226498. [PubMed: 30733314]

Bartlett EA, Ananth M, Rossano S, et al. , 2019. Quantification of positron emission tomography data using simultaneous estimation of the input function: validation with venous blood and replication of clinical studies. Mol. ImAging Biol 21 (5), 926–934. 10.1007/s11307-018-1300-1. [PubMed: 30535672]

Bartlett EA, Ogden RT, Mann JJ, Zanderigo F, 2022. Source-to-target automatic rotating estimation (STARE) – A publicly-available, blood-free quantification approach for PET tracers with irreversible kinetics: theoretical framework and validation for [18F]FDG. Neuroimage 249, 118901. 10.1016/j.neuroimage.2022.118901. [PubMed: 35026425]

Catana C., 2019. Development of dedicated brain PET imaging devices: recent advances and future perspectives. J. Nucl. Med 60 (8), 1044–1052. 10.2967/jnumed.118.217901. [PubMed: 31028166]

Cherry SR, Jones T, Karp JS, Qi J, Moses WW, Badawi RD, 2018. Total-body PET: maximizing sensitivity to create new opportunities for clinical research and patient care. J. Nucl. Med 59 (1), 3–12. 10.2967/jnumed.116.184028. [PubMed: 28935835]

Croteau E, Lavallée É, Labbe SM, et al. , 2010. Image-derived input function in dynamic human PET/CT: methodology and validation with 11C-acetate and 18F-fluorothioheptadecanoic acid in muscle and 18F-fluorodeoxyglucose in brain. Eur. J. Nucl. Med. Mol. Imaging 37 (8), 1539–1550. 10.1007/s00259-010-1443-z. [PubMed: 20437239]

de, Geus-Oei LF, Visser EP, Krabbe PFM, et al. , 2006. Comparison of image-derived and arterial input functions for estimating the rate of glucose metabolism in therapy-monitoring 18F-FDG PET studies. J. Nucl. Med 47 (6), 945–949. [PubMed: 16741303]

van der, Weerdt AP, Klein LJ, Boellaard R, Visser CA, Visser FC, Lammertsma AA, 2001. Image-derived input functions for determination of MRGlu in cardiac 18F-FDG PET scans. J. Nucl. Med 42 (11), 1622–1629. [PubMed: 11696630]

Dimitrakopoulou-Strauss A, Pan L, Sachpekidis C, 2021. Kinetic modeling and parametric imaging with dynamic PET for oncological applications: general considerations, current clinical applications, and future perspectives. Eur. J. Nucl. Med. Mol. ImAging 48 (1), 21–39. 10.1007/s00259-020-04843-6. [PubMed: 32430580]

Eberl S, Anayat AR, Fulton RR, Hooper PK, Fulham MJ, 1997. Evaluation of two population-based input functions for quantitative neurological FDG PET studies. Eur. J. Nucl. Med 24 (3), 299–304. 10.1007/BF01728767. [PubMed: 9143468]

Feng D, Wang X, Yan H, 1994. A computer simulation study on the input function sampling schedules in tracer kinetic modeling with positron emission tomography (PET). Comput. Methods Programs Biomed 45 (3), 175–186. 10.1016/0169-2607(94)90201-1. [PubMed: 7705075]

Feng D, Wong KP, Wu CM, Siu WC, 1997. A technique for extracting physiological parameters and the required input function simultaneously from PET image measurements: theory and simulation study. IEEE Trans. Inf. Technol. Biomed 1 (4), 243–254. 10.1109/4233.681168. [PubMed: 11020827]

Feng ST, Cui M, Gao J, Wu B, Sha W, Huang B, 2012. Image-derived arterial input function in dynamic positron emission tomography–computed tomography: a method using both positron emission tomographic and computed tomographic images. J. Comput. Assist. Tomogr 36 (6), 762. 10.1097/RCT.0b013e31826bdd09. [PubMed: 23192217]

Feng DD, Chen K, Wen L, 2020. Noninvasive input function acquisition and simultaneous estimations with physiological parameters for PET quantification: a brief review. IEEE Trans. Radiat. Plasma Med. Sci 4 (6), 676–683. 10.1109/TRPMS.2020.3010844.

Gallezot JD, Lu Y, Naganawa M, Carson RE, 2020. Parametric imaging with PET and SPECT. IEEE Trans. Radiat. Plasma Med. Sci 4 (1), 1–23. 10.1109/TRPMS.2019.2908633.

Guo H, Renaut RA, Chen K, 2007. An input function estimation method for FDG-PET human brain studies. Nucl. Med. Biol 34 (5), 483–492. 10.1016/j.nucmedbio.2007.03.008. [PubMed: 17591548]

Kolanko MA, Win Z, Loreto F, et al. , 2020. Amyloid PET imaging in clinical practice. Pract. Neurol 20 (6), 451–462. 10.1136/practneurol-2019-002468. [PubMed: 32973035]

Landau SM, Thomas BA, Thurfjell L, et al. , 2014. Amyloid PET imaging in Alzheimer's disease: a comparison of three radiotracers. Eur. J. Nucl. Med. Mol. ImAging 41 (7), 1398–1407. 10.1007/s00259-014-2753-3. [PubMed: 24647577]

Loening AM, Gambhir SS, 2003. AMIDE: a free software tool for multimodality medical image analysis. Mol. ImAging 2 (3), 15353500200303133. 10.1162/15353500200303133.

Mourik JEM, Lubberink M, Klumpers UMH, Comans EF, Lammertsma AA, Boellaard R, 2008. Partial volume corrected image derived input functions for dynamic PET brain studies: methodology and validation for [11C]flumazenil. Neuroimage 39 (3), 1041–1050. 10.1016/j.neuroimage.2007.10.022. [PubMed: 18042494]

Naganawa M, Gallezot JD, Shah V, et al. , 2020. Assessment of population-based input functions for Patlak imaging of whole body dynamic 18F-FDG PET. EJNMMI. Phys 7 (1), 67. 10.1186/s40658-020-00330-x. [PubMed: 33226522]

Ogden RT, Zanderigo F, Choy S, Mann JJ, Parsey RV, 2010. Simultaneous estimation of input functions: an empirical study. J. Cereb. Blood Flow Metab 30 (4), 816–826. 10.1038/jcbfm.2009.245. [PubMed: 19997119]

Okamura N, Harada R, Ishiki A, Kikuchi A, Nakamura T, Kudo Y, 2018. The development and validation of tau PET tracers: current status and future directions. Clin. Transl. ImAging 6 (4), 305–316. 10.1007/s40336-018-0290-y. [PubMed: 30148121]

Providência L, Weijden CWJ van der, Mohr P, et al. , 2024. Can internal carotid arteries be used for noninvasive quantification of brain PET studies? J. Nucl. Med 10.2967/jnumed.123.266675. Published online March 14.

Riabkov DY, Bella EVRD, 2004. Blind identification of the kinetic parameters in three-compartment models. Phys. Med. Biol 49 (5), 639. 10.1088/0031-9155/49/5/001. [PubMed: 15070194]

Riabkov DY, Di Bella EVR, 2002. Estimation of kinetic parameters without input functions: analysis of three methods for multichannel blind identification. IEEE Trans. Biomed. Eng 49 (11), 1318–1327. 10.1109/TBME.2002.804588. [PubMed: 12450362]

Saint-Aubert L, Lemoine L, Chiotis K, Leuzy A, Rodriguez-Vieitez E, Nordberg A, 2017. Tau PET imaging: present and future directions. Mol. Neurodegener 12 (1), 19. 10.1186/s13024-017-0162-3. [PubMed: 28219440]

Samil Yetik I, Qi J, 2006. Direct estimation of kinetic parameters from the sinogram with an unknown blood function. In: 3rd IEEE International Symposium on Biomedical Imaging: Nano to Macro, 2006, pp. 295–298. 10.1109/ISBI.2006.1624911.

Sari H, Erlandsson K, Marner L, et al. , 2018. Non-invasive kinetic modelling of PET tracers with radiometabolites using a constrained simultaneous estimation method: evaluation with 11C-SB201745. EJNMMI. Res 8 (1), 58. 10.1186/s13550-018-0412-6. [PubMed: 29971517]

Spencer BA, Berg E, Schmall JP, et al. , 2020. Performance evaluation of the uEXPLORER Total-body PET/CT scanner based on NEMA NU 2-2018 with additional tests to characterize long axial field-of-view PET scanners. J. Nucl. Med 10.2967/jnumed.120.250597. Published online October 1.

Strauss LG, Klippel S, Pan L, Schönleben K, Haberkorn U, Dimitrakopoulou-Strauss A, 2007. Assessment of quantitative FDG PET data in primary colorectal tumours: which parameters are important with respect to tumour detection? Eur. J. Nucl. Med. Mol. ImAging 34 (6), 868–877. 10.1007/s00259-006-0319-8. [PubMed: 17219134]

Takikawa S, Dhawan V, Spetsieris P, et al. , 1993. Noninvasive quantitative fluorodeoxyglucose PET studies with an estimated input function derived from a population-based arterial blood curve. Radiology 188 (1), 131–136. 10.1148/radiology.188.1.8511286. [PubMed: 8511286]

Thorwarth D, Eschmann SM, Scheiderbauer J, Paulsen F, Alber M, 2005. Kinetic analysis of dynamic 18F-fluoromisonidazole PET correlates with radiation treatment outcome in head-and-neck cancer. BMC Cancer 5 (1), 152. 10.1186/1471-2407-5-152. [PubMed: 16321146]

van der Weijden CWJ, Mossel P, Bartels AL, et al. , 2023. Non-invasive kinetic modelling approaches for quantitative analysis of brain PET studies. Eur. J. Nucl. Med. Mol. ImAging 50 (6), 1636–1650. 10.1007/s00259-022-06057-4. [PubMed: 36651951]

Volpi T, Maccioni L, Colpo M, et al. , 2023. An update on the use of image-derived input functions for human PET studies: new hopes or old illusions? EJNMMI Res. 13 (1), 97. 10.1186/s13550-023-01050-w. [PubMed: 37947880]

Wahl LM, Asselin MC, Nahmias C, 1999. Regions of interest in the venous sinuses as input functions for quantitative PET. J. Nucl. Med 40 (10), 1666–1675. [PubMed: 10520707]

Wang G, Qi J, 2015. PET image reconstruction using kernel method. IEEE Trans. Med. ImAging 34 (1), 61–71. 10.1109/TMI.2014.2343916. [PubMed: 25095249]

Wang G, Rahmim A, Gunn RN, 2020. PET parametric imaging: past, present, and future. IEEE Trans. Radiat. Plasma Med. Sci 4 (6), 663–675. 10.1109/TRPMS.2020.3025086. [PubMed: 33763624]

Wang G, Nardo L, Parikh M, et al. , 2022. Total-body PET multiparametric imaging of cancer using a voxelwise strategy of compartmental modeling. J. Nucl. Med 63 (8), 1274–1281. 10.2967/jnumed.121.262668. [PubMed: 34795014]

Wang G., 2019. High temporal-resolution dynamic PET image reconstruction using a new spatiotemporal kernel method. IEEE Trans. Med. ImAging 38 (3), 664–674. 10.1109/TMI.2018.2869868. [PubMed: 30222553]

Wong KP, Meikle SR, Feng D, Fulham MJ, 2002. Estimation of input function and kinetic parameters using simulated annealing: application in a flow model. IEEE Trans. Nucl. Sci 49 (3), 707–713. 10.1109/TNS.2002.1039552.

Wong KP, Huang SC, Fulham MJ, 2006. Evaluation of an input function model that incorporates the injection schedule in FDG-PET studies. In: 2006 IEEE Nuclear Science Symposium Conference Record, pp. 2086–2090. 10.1109/NSSMIC.2006.354325. Vol 4.

Yi-Gen W., 2008. Noninvasive quantification of local cerebral metabolic rate of glucose for clinical application using positron emission tomography and 18F-fluoro-2-deoxy-D-glucose. J. Cereb. Blood Flow Metab 28 (2), 242–250. 10.1038/sj.jcbfm.9600535. [PubMed: 17684521]

Zanderigo F, D'Agostino AE, Joshi N, et al. , 2018. [11C]Harmine binding to brain monoamine oxidase a: test-retest properties and noninvasive quantification. Mol. ImAging Biol 20 (4), 667–681. 10.1007/s11307-018-1165-3. [PubMed: 29423903]

Zanotti-Fregonara P, Fadaili EM, Maroy R, et al. , 2009. Comparison of eight methods for the estimation of the image-derived input function in dynamic [18F]-FDG PET human brain studies. J. Cereb. Blood Flow Metab 29 (11), 1825–1835. 10.1038/jcbfm.2009.93. [PubMed: 19584890]

Zanotti-Fregonara P, Liow JS, Fujita M, et al. , 2011. Image-derived input function for human brain using high resolution PET imaging with [11C](R)-rolipram and [11C]PBR28. PLoS One 6 (2), e17056. 10.1371/journal.pone.0017056. [PubMed: 21364880]

Zhang X, Xie Z, Berg E, et al. , 2020. Total-body dynamic reconstruction and parametric imaging on the uEXPLORER. J. Nucl. Med 61 (2), 285–291. 10.2967/jnumed.119.230565. [PubMed: 31302637]

Zuo Y, Qi J, Wang G, 2018. Relative patlak plot for dynamic PET parametric imaging without the need for early-time input function. Phys. Med. Biol 63 (16), 165004 10.1088/1361-6560/aad444. [PubMed: 30020080]

Zuo Y, López JE, Smith TW, et al. , 2021. Multiparametric cardiac 18F-FDG PET in humans: pilot comparison of FDG delivery rate with 82Rb myocardial blood flow. Phys. Med. Biol 66 (15), 155015 10.1088/1361-6560/ac15a6.

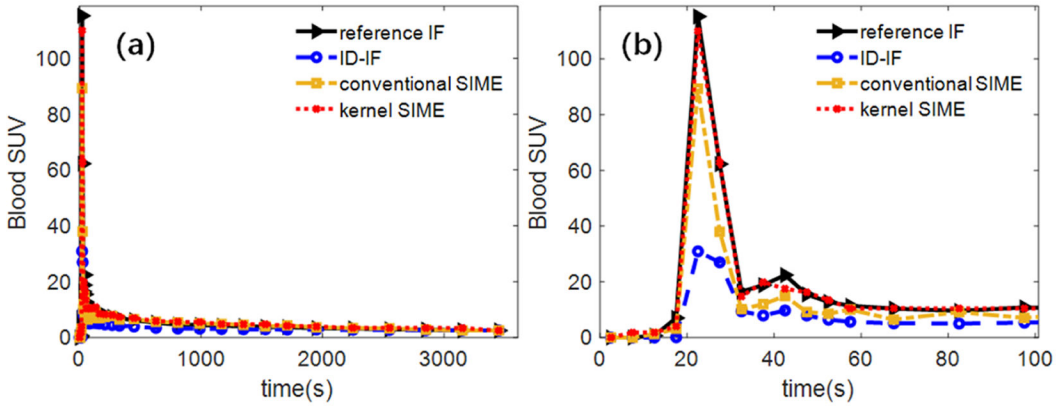

Fig. 1.

Estimated input functions by different methods used in the simulation study. (a) 0–60 min. (b) zoomed-in plots for 0–100 s.

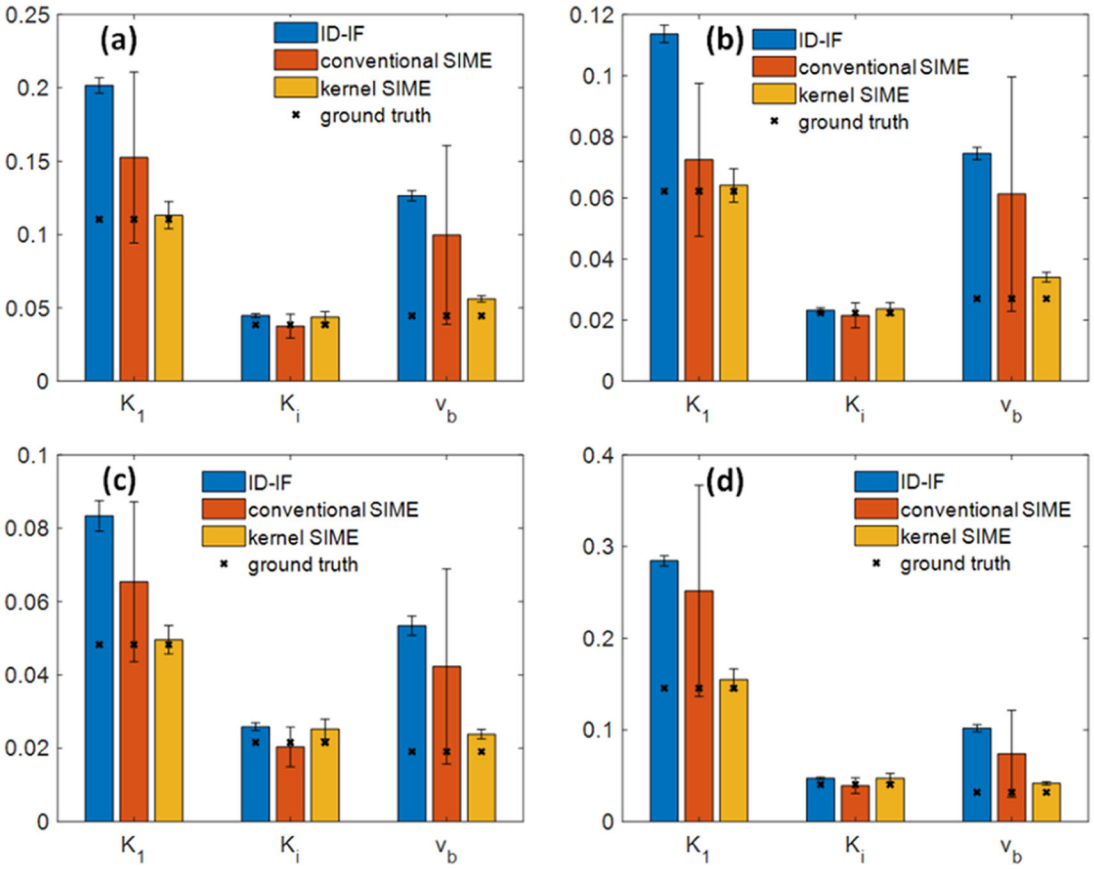

Fig. 2.

Estimated kinetic parameters of brain regions using the input function derived from different methods in the simulation study in (a) GM, (b) WM, (c) CSF, and (d) cerebellum. The error bars indicate the standard deviations of the estimated parameters. .

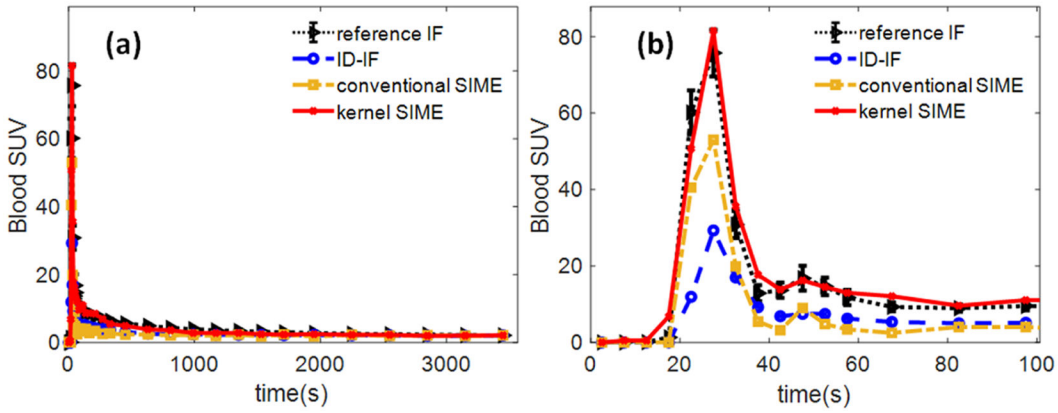

Fig. 3.

Estimated input functions by different methods in the human-subject study. (a) 0–60 min. (b) zoomed-in plots for 0–100 s. The error bars on the reference IF indicate the standard deviation of blood SUV within the ascending aorta region.

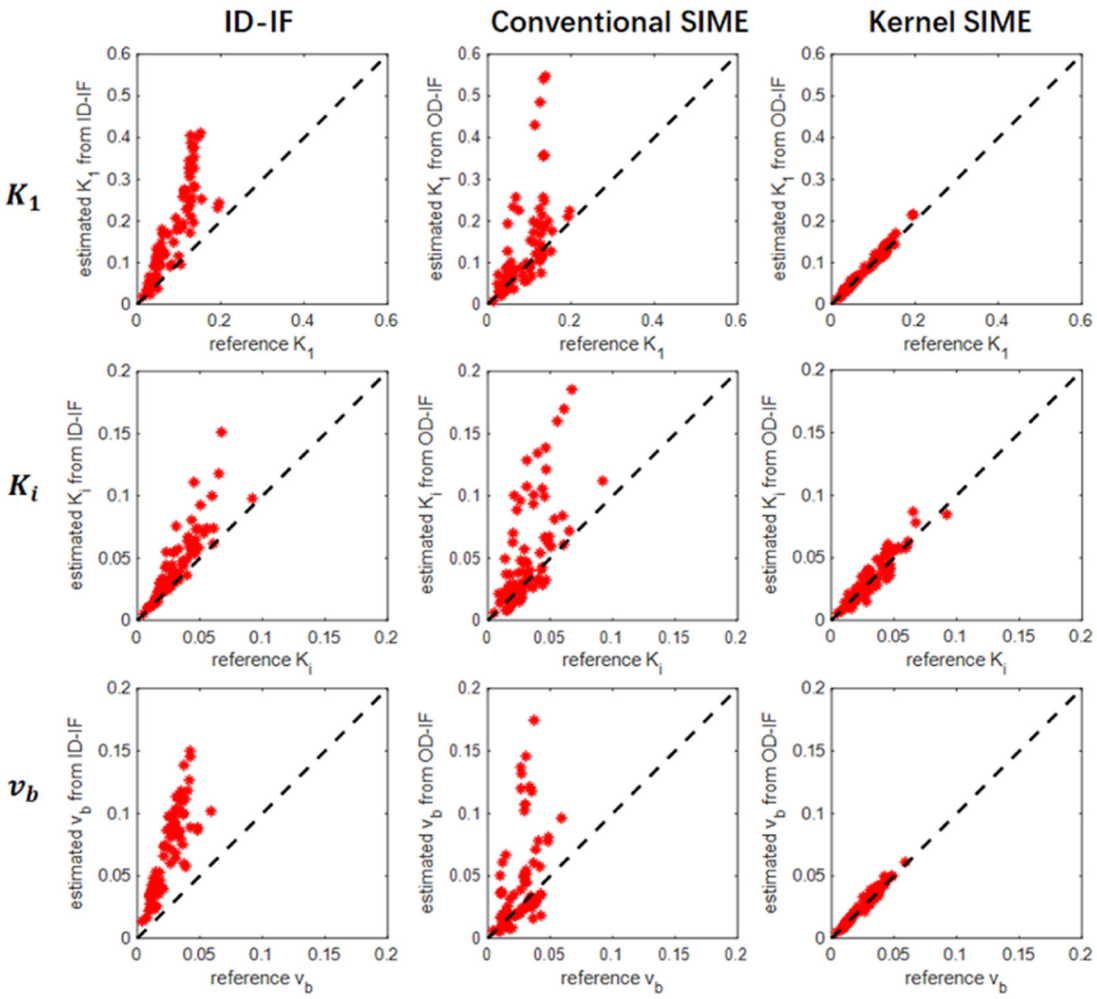

Fig. 4.

Scatter plot of the estimated kinetic parameters vs. reference kinetic parameters. The black dashed line indicates the case that the estimated parameter is equal to the reference value. Each dot represents an estimated kinetic parameter from one brain region (GM, WM, CSF, cerebellum) of one human subject.

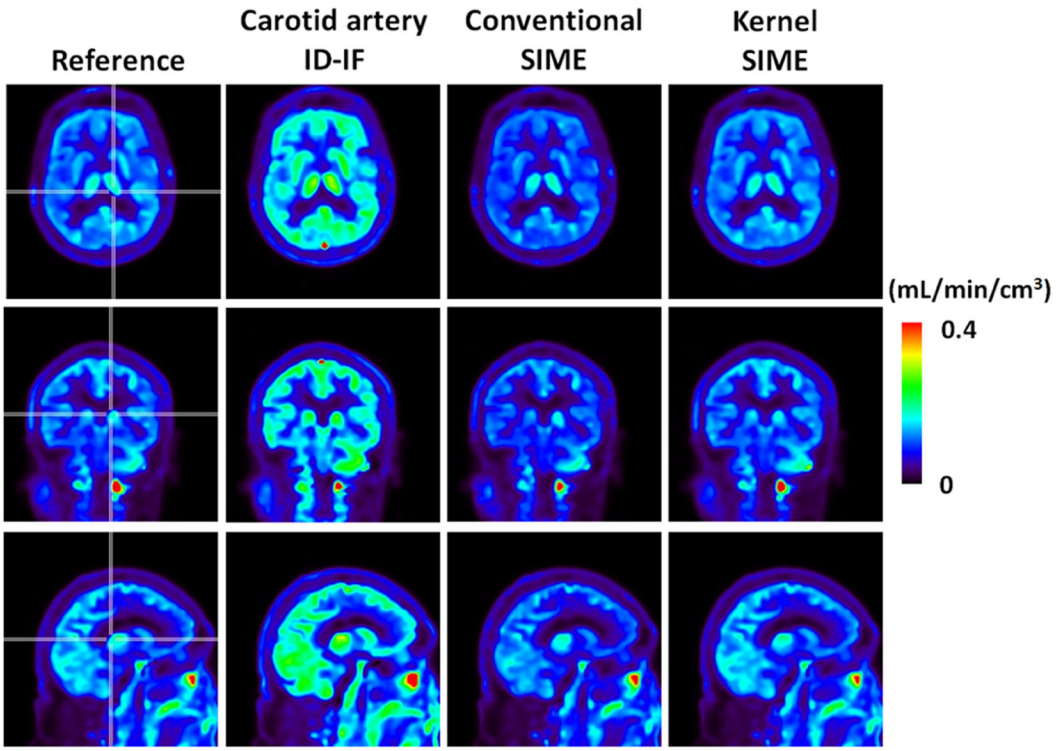

Fig. 5.

Transverse (top row), coronal (middle row) and sagittal (bottom row) views of K_1 images of brain generated with the input functions by different methods.

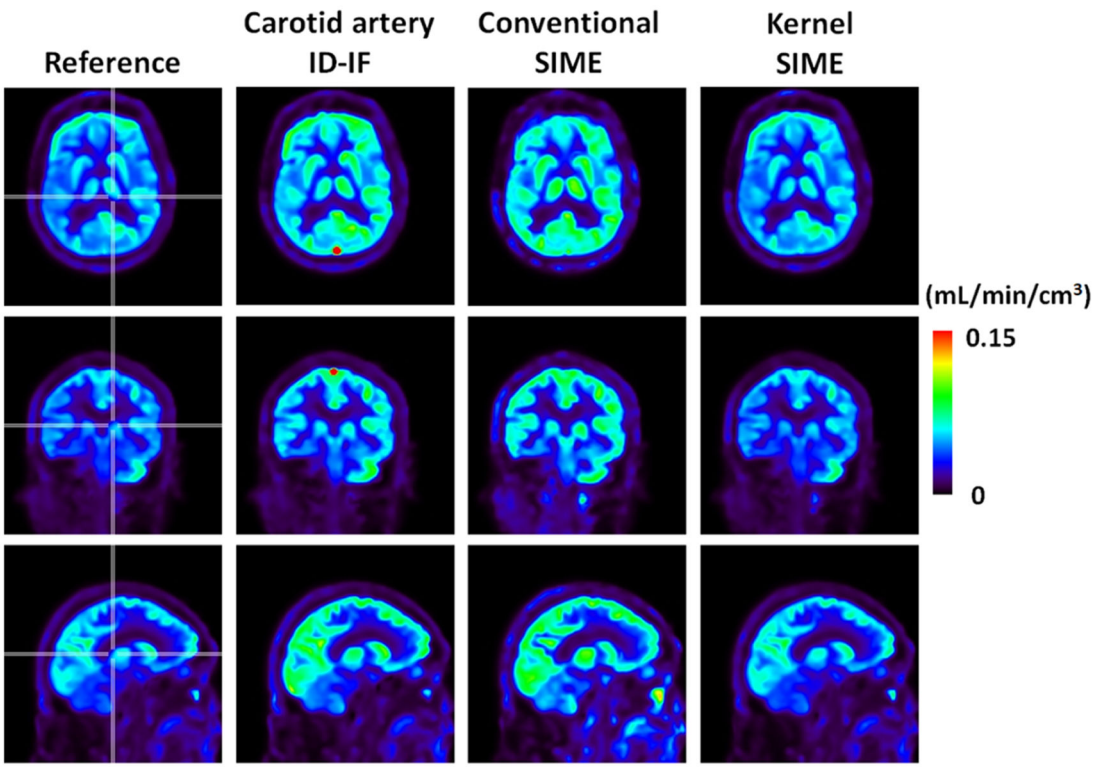

Fig. 6.

Transverse (top row), coronal (middle row) and sagittal (bottom row) views of K_i images of brain generated with the input functions by different methods.

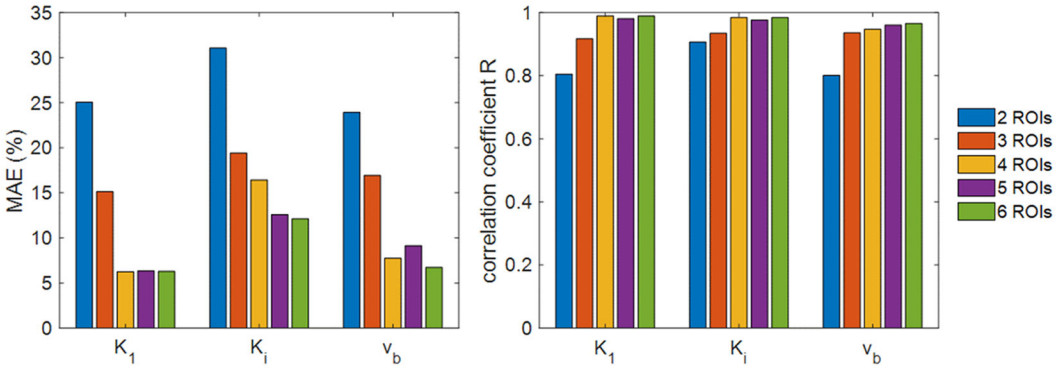

Fig. 7.

Effect of the number of used ROIs in the kernel SIME on the performance of kinetic parameter quantification. Left: MAEs and right: Pearson correlation coefficients.

Table 1

Kinetic parameters set in the simulation study.

	v_b	K_1 (mL/min/cm^3)	k_2(min^{-1})	k_3(min^{-1})	k_4(min^{-1})
GM	0.045	0.110	0.191	0.102	0.009
WM	0.027	0.062	0.125	0.070	0.010
CSF	0.019	0.048	0.215	0.174	0.019
Cerebellum	0.032	0.146	0.231	0.089	0.007

Table 2

Demographic characteristics of healthy subjects and cancer patients.

	Healthy subjects	Cancer patients
Number of Subjects	10	10
Age (years) [mean ± SD]	50 ± 15	69 ± 8
Sex (male/female)	8/2	4/6
Body mass index (kg/m^2) [mean ± SD]	29.1 ± 5.9	25.4 ± 5.2

Table 3

MAE and correlation coefficient R of the estimated kinetic parameters for human-subject dataset.

	ID-IF		Conventional SIME		Kernel SIME	
	MAE	**R**	**MAE**	**R**	**MAE**	**R**
K_1	101.2 %	0.86	65.8 %	0.61	6.8 %	0.99
K_i	37.1 %	0.87	77.6 %	0.65	16.3 %	0.98
v_b	186.2 %	0.85	92.7 %	0.46	8.3 %	0.94